A Systematic Study of Jet Quenching via 3 Particle Angular Correlations

Chris Rosen, Dept. of Physics

Committee Members

Thesis Advisor: Dr. Jamie Nagle, Department of Physics

Dr. John Cumalat, Department of Physics

Dr. Valerie Otero, School of Education

Department of Physics

April 12, 2006

Abstract

Recent studies of hadron jets from heavy ion collisions seem to suggest that the produced matter alters the jets in a characteristic way. Understanding this modification mechanism may reveal new properties of the produced matter, such as it's speed of sound or resistance to flow. In this work, I develop simple models of two competing methods of jet modification, and present a simulation of these altered jets in the PHENIX experiment. I find that the acceptance of the drift chambers in PHENIX has a notable influence on three particle correlation histograms, and comment on the feasibility of resolving bent and conical jets by way of angular correlations. I show that three particle angular correlations result in distinct features of a conical jet that differ from those of a bent jet, and that the detector's acceptance unfavorably alters these features. I conclude with some remarks on the simulation's utility, as well as how it might be improved.

Acknowledgments

There is no doubt in my mind that this project has been the most meaningful aspect of my undergraduate adventure. Over the course of three semesters, I've learned a ton about the physics of elementary particles and heavy ion collisions, just as much about writing simulations, and more about expressing my scientific ideas. More than that, solving the correlation problems and understanding my simulation results was just *fun*. Above all else, I owe this phenomenal experience to my advisor, Dr. Jamie Nagle. Jamie provided invaluable suggestions, encouragement, and good old fashioned inspiration just about every step of the way. I am also indebted to Andrew Adare, Andy Glenn, and Matt Wysocki for their superb technical expertise. Without their patience and support, I'd probably still find myself working out the complexities of "hello_world.cc". Finally I would like to thank Morgan Newberg for sacrificing her weekends to shuttle me to and from the lab, and everybody else who offered comments of any kind on this project.

Contents

Chapter 1

A Physics Overview

1.1 What's the Matter?

The world we live in today is thought to be composed of a handful of elementary particles subjected to even fewer governing forces. These particles can arrange themselves into a variety of atoms, which are carefully tabulated by way of a Periodic Table. In turn, these atoms can join to form molecules which arrange themselves into different states of matter (such as solids, liquids, and gases) and these states of matter can even transition from one to another.

But was this always the case? One very interesting question in physics asks whether or not the atoms and particles of today arrange themselves in the same ways as particles and atoms did billions of years ago. In an attempt to answer this question, one can step backward through time and examine how the changing conditions of our universe affected the matter within it.

About 400,000 years after the universe popped into existence by way of the big bang, electrons and nucleons joined together, forming atoms in a process known as recombination. Before this, the universe was sufficiently hot that electrons had enough energy to overcome

the electromagnetic attraction of the protons and travel freely through the universe. The photons previously trapped in a dense sea of electrically charged particles are suddenly released, and travel out from the scattering trap in all directions creating the cosmic microwave background still visible today.

5 seconds after the big bang, amidst a collection of speeding photons and electrons, the universe has cooled enough to allow once unbound neutrons and protons to feel the effects of the strong force. This short range force secures the two to one another in the process called nucleosynthesis. Previously, lone protons and neutrons (themselves composite objects of three confined quarks) ignored each other, and there was some chance that an unbound neutron could decay. [1]

The current theory of quarks and their interactions, quantum chromodynamics (QCD), predicts that at a high enough energy density, a new state of matter will be formed in which quarks and gluons (the gauge bosons of the strong force) are *deconfined* from one another. These were precisely the conditions of the early universe until about one microsecond after the big bang.

This new state of matter, the quark-gluon plasma (QGP), represents an interesting puzzle that may offer a test of our knowledge about the way quarks and gluons interact. In the following sections I will provide an overview of one experiment capable of seeing a quark-gluon plasma for the first time in over 15 billion years, as well as a quick discussion of the big ideas in QCD and their experimental implications.

1.2 A Big Bang of Our Own

In order to replicate the conditions present in the first moments of our universe's existence, one must find a way to put a lot of energy into a very small space. One good way to do this

[1] The lifetime of an unbound neutron is around 885 seconds, or something like 15 minutes [1].

is to collide two tiny particles that are given a large kinetic energy.

Since the kinetic energy of a particle depends on both the particle's mass as well as it's speed, the ideal collision takes place between two heavy particles traveling extraordinarily fast. At Brookhaven National labs in New York, the Relativistic Heavy Ion Collider (RHIC) accelerates gold nuclei to more than 99.9% the speed of light and slams them into one another, creating a region of extraordinarily high energy density within the collider. This region earns the appropriate title of "the fireball", and is characterized by an energy density in excess of 5 GeV/fm^3 [2].

The experiment uses gold ions for two fundamental reasons. First, gold nuclei are largely spherical in shape, which simplifies the collision analysis. Furthermore, with 79 protons and 118 neutrons, these ions have a sufficiently large mass. Since the collider is capable of creating collisions with a nucleon-nucleon center of mass energy around $\sqrt{s_{NN}} = 200$ GeV, these Au-Au collisions are capable of producing upwards of 40 TeV.

When the two gold nuclei collide, the extremely high energy density ensures that there is a high volume of produced matter that travels from the fireball in such a way that both energy and momentum are conserved. These newly created particles can be tracked and identified by any number of detectors surrounding the beampipe. From these detectors, one can gain knowledge about both the types of particles emerging from the collision, as well as the kinematics of the particles, such as their energies and momenta. With this information, one can hope to work backwards, reconstructing the event and understanding the collision details.

One of the four groups studying these collisions at RHIC is PHENIX, or the **P**ioneering **H**igh **E**nergy **N**uclear **I**nteraction e**X**periment. PHENIX is currently the largest experiment taking data at the RHIC, and one of its principle objectives is to determine whether or not a quark-gluon plasma is being created in heavy ion collisions. In order to accomplish this, PHENIX is designed to measure direct probes of the nuclear collisions—particles like photons

and muons that are produced as a result of the collision. More specifically, PHENIX uses the dilepton pairs (like $\mu^{\pm}$) to determine whether or not the properties of decaying vector mesons (such as the J/ψ) are altered by the collision. PHENIX also has the ability to measure the trajectories and momenta of charged hadrons by way of a drift chamber. This particular detector will be of some importance to this work, and I will return to it in detail at the start of chapter 3.

1.3 A Colorful Theory

In order to better understand the scientific ramifications of a quark-gluon plasma, it may be helpful to discuss some of the defining characteristics of quark-gluon interactions. To begin, there are six known quarks conveniently arranged into three doublets, like

$$\begin{pmatrix} u \\ d \end{pmatrix}, \quad \begin{pmatrix} c \\ s \end{pmatrix}, \quad \begin{pmatrix} t \\ b \end{pmatrix}$$

where the upper quark in each doublet has charge $+2/3$ and the lower $-1/3$ in units of fundamental charge, e. For every quark there is also an anti-quark, with the same mass and opposite charge. Quarks group themselves in one of two specific ways to create particles known as hadrons. They can either form a group of three, creating the baryons (protons, neutrons, etc.) or groups of two with one quark and one anti quark. The latter are known as mesons, examples of which are the π^0 and the J/ψ. As an example, the quarks in the first doublet, u ("up") and d ("down") combine to create the protons (uud) and neutrons (udd) that make up the nuclei of every known element.

In addition to the electric charge carried by each quark, there is also a "color charge" which enables the quarks to participate in the strong interactions. There are three different types of color charge, and they are traditionally labeled red, green, and blue. It is an

experimentally determined truth that every naturally occurring (observable) hadron is a color singlet. In analogy with color addition in light, this is one way of saying that every baryon contains one red, one green and one blue quark (Red + Green + Blue = White) and every meson is a combination of color/anti-color quark/anti-quarks (Red + Anti-Red = White).

The theory of the strong interaction, QCD, fits nicely into the special unitary group $SU(3)$, with the red, green, blue triplet as the fundamental representation. The group has eight generators, and since they do not all commute, QCD is a non-Abelian gauge theory. In QCD, the gauge boson is the gluon, a massless spin one particle that can be thought of as the force carrier of the strong interaction. Gluons themselves have color charge, in fact each gluon carries one unit of color and one unit of anti-color. This curiosity gives QCD many of its unique properties. Most importantly, since the gluons carry color charge, they can couple to one another in three and four gluon vertexes known as "glue-balls".

Another interesting consequence of the gluon self-coupling arises when one attempts to determine the strength of the interaction between two quarks. By way of analogy, consider first the Coulomb interaction between two (electrically) charged particles. Because the strength of the Coulomb interaction drops off as $1/r^2$ the lines of interaction between the two particles get farther and farther apart as one moves away from the system (figure 1.1, left). The strong interaction, by contrast, is quite different. If one brings two, say, green quarks very near one another, the apparent color charge will decrease by way of a sort of anti-screening mechanism. This oddity results in the so called "asymptotic freedom" of the quarks—when they are very close together they essentially act like free particles.

Now we can consider what happens when one tries to pull a quark (q) and an anti-quark ($\bar{q}$) farther apart from one another. Because the gluons themselves are colored, one can think of the interaction lines between the $q\bar{q}$ pair as having some attraction to *each other*. This effectively groups all the interaction lines into a bundle of parallel lines known as a flux tube,

describing a force independent of the quark's spatial separation (figure 1.1, right). Another way of saying this is that the potential between the two quarks increases linearly with the distance between them.

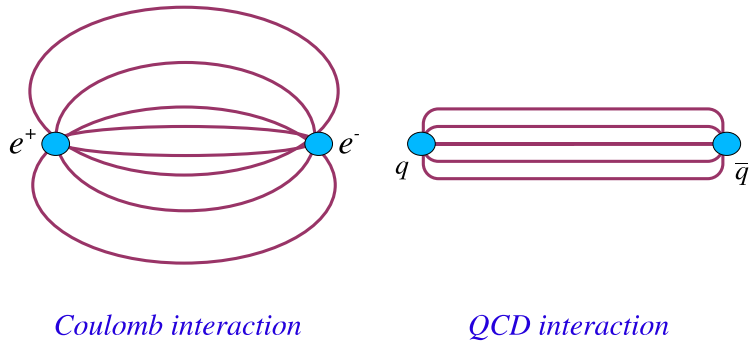

Figure 1.1: Two sketches showing the differences between the Coulomb interaction (between e^-e^+) and the strong (QCD) interaction (between $q\bar{q}$). The interaction lines representing the Coulomb force are free to spread out in space, and they do so in such away that their density decreases like $1/r^2$. For the strong interaction, the lines are effectively attracted to one another resulting in the flux tube shown above and a linear potential.

In the context of heavy ion collisions, this effective potential has some rather profound implications. Most notably, it is interesting to ask what happens when the quarks in the above paragraph are stretched farther and farther apart. As the quark and anti-quark separate, the color field between them grows larger and larger until they are separated by about 10^{-15} m, the typical diameter of a hadron. At this point it is energetically favorable for new $q\bar{q}$ pairs to pop out of the vacuum and form mesons and baryons with the existing quark and anti-quark. This process continues as long as it costs less energy than the rest mass of the new quarks and the energy of separation between the $q\bar{q}$ pairs. The newly formed hadrons carry with them some energy and momentum from the original $q\bar{q}$ separation, and so

they too travel from the point of separation in back to back streams of mesons and baryons. For somewhat intuitive reasons, these streams of particles are known as jets.

From the preceding paragraphs, it should now be clear why a QGP is of substantial scientific interest. Primarily, the observation that all naturally occurring particles are contained in "white" color singlets, alongside the interesting quark interaction that forbids a quark and anti-quark from being pulled apart farther than a Fermi, can be summarized by saying that quarks and gluons are *confined*. Under everyday conditions, neither a quark nor a gluon will ever be found unaccompanied by other quarks and gluons. In this respect, if an experiment such as PHENIX succeeds in identifying a plasma composed of deconfined quarks and gluons, scientists will have access to a state of matter that last existed microseconds after the big bang, when the conditions were far from 'everyday'.

Chapter 2

Toward an Understanding of Fireball Physics

2.1 Jets as a Diagnostic Tool

The hadron jets produced in heavy ion collisions turn out to be one of the most useful probes in determining the properties of the quark-gluon plasma. As the stream of partons (quarks and gluons) produced by $q\bar{q}$ separation traverse the fireball, the highly energetic matter alters the jet path in a characteristic way. By studying these path alterations, it is possible to discover some interesting properties of the QGP, such as it's resistance to flow.

It is easy to understand this phenomenon by way of analogy: Imagine yourself shooting a bullet through a swimming pool filled with an unknown substance. From experience, you know that a bullet fired in ordinary air should travel with some velocity, v, and in a relatively straight line from the muzzle of your weapon. When you shoot the gun through the mystery matter in the swimming pool, however, something very different happens. Instead of traveling at it's characteristic velocity, you find that the bullet traveled much slower—$v/10$. Additionally, instead of striking the other side of the pool at a point in front of the gun, the

bullet ended up 20 yards to the left.

With these results, one can begin to ask important questions about the unknown substance. Is it uniform? What happens when I shoot ten bullets from ten different locations? Do they always end up 20 yards to the left? By comparing the behavior of the bullet in the mystery matter to predictions from a variety of models, one can hope for a better understanding of what's inside the pool.

The use of jets in the study of heavy ion collisions is similar in many ways. When a jet is produced, the energetic partons leave the original $q\bar{q}$ pair in opposing (back-to-back) directions in such a way as to conserve momentum and energy. In empty space, the transverse momentum, p_T (the momentum perpendicular to the beam pipe), of particles in both sides of the jet should be about the same. If, however, the $q\bar{q}$ pair begins to separate near the edge of the fireball, the situation is quite different (Figure 2.1). In this case, the partons in the jet traveling toward the nearby surface may emerge with higher transverse momentum than the opposing jet, which is forced to travel through most of the fireball. As the partons travel through the fireball, they deposit most (if not all) of their energy and momentum into the matter produced by the collision [3]. This phenomena is known as jet quenching, and it

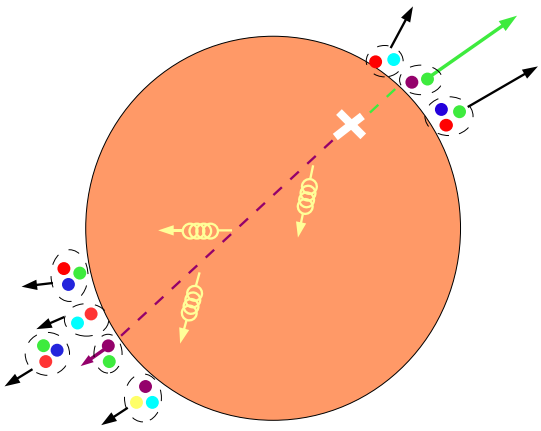

Figure 2.1: Sketch of the fireball (orange) inside a heavy ion collision. X marks the spot of $q\bar{q}$ separation, and arrows indicate magnitude of hadron p_T. Particles that traverse much of the fireball give up most of their energy and momentum and lead to jet quenching.

lies at the heart of QGP study.

2.1.1 The Correlation Scheme

In order to study this jet quenching, it is helpful to utilize two and three particle angular correlations. In this technique, one studies the angular distribution between some trigger particle in a jet and one or two associated jet particles (respectively). To make this method meaningful in the study of heavy ion collisions, one can choose the trigger particle to be one of the high p_T hadrons that does not leave much energy or momentum in the QGP. This choice increases the probability that jet particles opposite the high p_T trigger have traveled a substantial distance through the energetically dense matter. In other words, these associated particles have had ample opportunity to be pushed around in some characteristic way by the QGP.

An important quantity in angular correlations is $\Delta\phi$, the azimuthal angle between the trigger particle and an associated (secondary) particle. If one considers a simple jet composed of two streams of hadrons back-to-back, then one would expect a one dimensional histogram to show peaks around $\Delta\phi = 0$ and π (for example, the blue line in figure 2.2). Any deviation in this distribution suggests a more complex jet geometry, and indicates particle path modification by the fireball.

2.2 Not Quite as Easy as π

In fact, the angular distribution obtained from particle correlations for Au+Au collisions is not peaked at both $\Delta\phi = 0$ and π. Instead, both PHENIX and STAR (another collaboration at the RHIC) have reported that the $\Delta\phi$ distribution for Au+Au collisions has a local *minimum* at $\Delta\phi = \pi$ with peaks on either side near $\pi \pm 1$ [3],[4]. A particularly illustrative plot of this result is shown in figure 2.2.

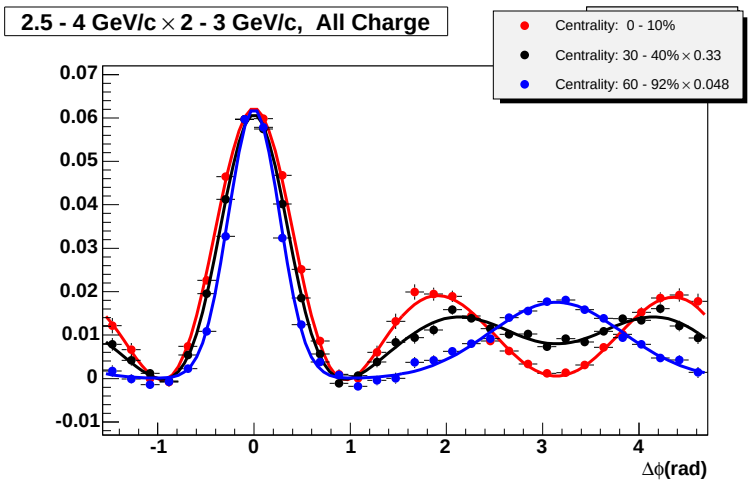

Figure 2.2: Plot showing the odd away side angular distribution. The peak at $\Delta\phi = 0$ contains the particles very near the high-p_T trigger, while the peaks on either side of $\Delta\phi = \pi$ count the secondaries. Notice the dependence on the centrality (how direct the collision between the gold nuclei). When centrality is low, the collision is more 'head-on' and one hopes for the production of a new state of matter. Plot from [5].

This curiosity has led to much speculation about the true geometry of the away-side jet. Recently, several models have appeared that attempt to describe the odd peaks in terms of bending, coherent gluon radiation, and collective excitation. In the following sections I will attempt to give a brief description of each.

2.2.1 Geometric Interlude

Before embarking on an investigation of the three primary models of jet modification, I would like to provide a quick explanation of how each will ultimately lead to the angular distribution shown in figure 2.2. In order to accomplish this, it will be necessary to know that geometrically, the three models are similar in one fundamental respect.

Ignoring the actual mechanism of the jet modification, two of the models predict that the associated particles lie on the surface of a cone. The remaining model suggests that the secondary particles follow a path that is "bent" from the trigger's axis by some angle. If the

associated particles can be bent in any direction, then (over many events) they too trace out the surface of a cone. [1] Most importantly, because both geometries effectively put particles on the circumference of a circle (a cone's cross section), they have the same map in $\Delta\phi$.

In an attempt to solidify this idea, I have provided the sketch in figure 2.3. This picture shows how particles that are very near the cone's opening angle in ϕ share very similar values of $\Delta\phi$. Conversely, the particles that are distributed near $\Delta\phi = \pi$ have very different values of $\Delta\phi$. In this way, even though the particles are effectively distributed randomly over the surface of a cone, they appear to "pile up" at the opening angle in the $\Delta\phi$ distributions.

[1] If this seems confusing, it may help to imagine holding both arms together in front of you at some angle toward the sky and spinning on your feet. As you do so, your arms will describe the surface of a cone.

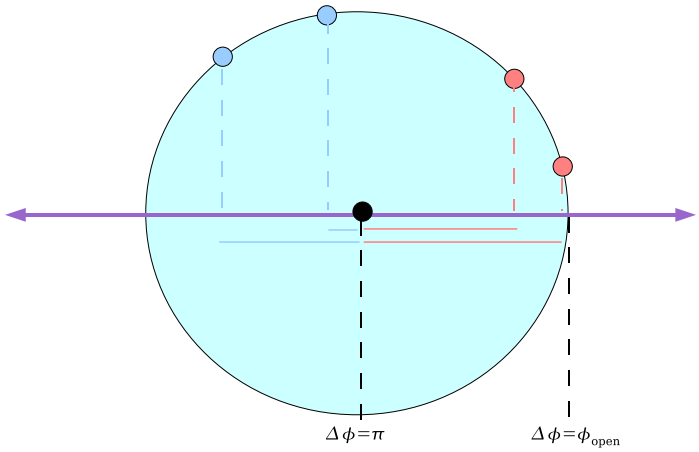

Figure 2.3: Picture attempting to show how all three models for jet modification could result in a histogram such as the one shown in figure 2.2. In this picture, $\Delta\phi$ is measured along the purple line. Notice how two particles along the "top" of the circle (light blue) have very different $\Delta\phi$ values (length of solid blue lines), while two the same distance apart but near the side (salmon) have very similar values of $\Delta\phi$ (length of salmon lines).

2.2.2 A Bent Jet

In the simplest of the three geometries, the two streams of hadrons are not back to back, but instead *bent*. The away-side jet (containing the hadrons that have traversed the fireball) is offset from the jet axis by an opening angle corresponding to the peak in the angular distribution. Since it is equally probable for the bent jet to open in any direction, one obtains peaks at both $\pi + \phi_{\text{open}}$ and $\pi - \phi_{\text{open}}$.

To bend a jet in this way, it has been suggested that the away-side jet receives a sort of shove from the flow of the produced matter [6]. When the ions collide, a collective flow field arises which has both longitudinal and transverse components with respect to the beam pipe. This flow field can interact with the partons in two distinct ways (figure 2.4). In the first case, the parton does not travel within the same Lorentz frame moving along the beampipe as the produced medium. This situation can arise as a result of either the point of production of the parton, or the time evolved trajectory of the medium. Most simply, nothing requires that the parton be produced in the same Lorentz frame as the medium. Furthermore, if the

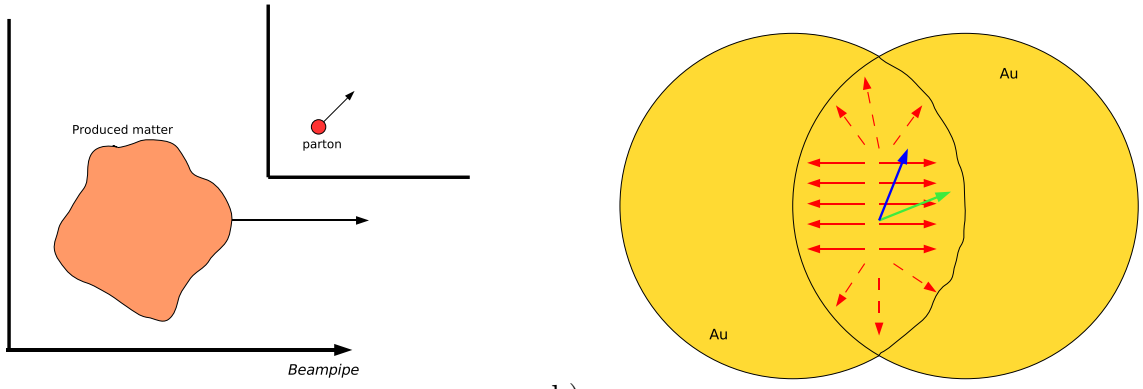

a) b)

Figure 2.4: Two scenarios describing the altered trajectory of partons by produced matter. In (a), where the parton is not in the Lorentz frame of the flow field, the longitudinal flow components push partons along the beampipe. In (b), hard partons traveling parallel to the collective flow (green) are favored, while those transverse (blue) can be muted. (Figure (b) adapted from [6])

parton *is* produced in the same frame as the medium, it will likely leave it. It's minuscule mass ensures that it will travel along a light-like line that generally intersects that of the collective flow field. For either of these scenarios, the end result is a bending of the jet in the direction of collective flow along the beampipe.

In the second case, the direction of the flow field directly modifies the parton's trajectory through the transfer of momentum. As a result of the collective flow, the momentum transfered to the parton does not depend on only the local energy density, but instead on the energy momentum tensor which contains contributions from the flow [6]. In this way, a small local energy density can still result in a sizable parton energy loss. More specifically, the low-p_T collective flow selects *against* hard partons traveling transverse to the direction of the flow field.

One hallmark of the bent jet scenario is that it is a relatively straightforward matter to distinguish between a bent jet and other, more complicated jet geometries. In particular, if a jet is indeed being bent by a flow field, all the particles in the jet should experience a similar path alteration. Accordingly, if one performs a three particle correlation, it should be true that the two low-p_T particles end up in the same peak in the $\Delta\phi$ distribution. Notice that in this case, two particle correlations fail to provide a distinction because it is equally likely that an associated particle can end up in either peak.

2.2.3 Radiating Gluons

Quite distinct from jet bending is the idea of a *cone* of secondary hadrons formed from the away side jet's interaction with the fireball. One possible mechanism of production for this geometry is Cherenkov-like gluon bremsstrahlung.

This scenario draws heavily from the QED analogue of Cherenkov radiation in a dielectric. Electrodynamicly, when a charged particle exceeds the speed of light in a dielectric, the material can emit a coherent cone of photons—the so-called Cherenkov radiation. Modern

high energy experiments routinely exploit this radiation for energetic particle detection. Another, more relevant means of obtaining Cherenkov radiation is the scattering of photons from a gas. Most importantly, this type of scattering will only produce Cherenkov radiation if the gas consists of bound states (such as atoms) and never from a gas of single elementary charged particles [7].

In this spirit, it may be possible to determine the interaction strength of the produced matter at the RHIC. If Cherenkov-like gluon radiation is observed in the heavy-ion collisions, it would indicate that the produced matter is comprised of some quark-gluon bound states. Additionally, it may be possible to investigate the resonance structure of these states and the nature of their interaction.

In the gluon radiation model (figure 2.5), a speeding gluon produced in a heavy-ion collision scatters from partonic bound states in the produced matter. In this process, the bound state may become excited and radiate a gluon as a result of the interaction. If the scattering conditions are such that the scattering amplitude is attractive, it is possible for the interaction to result in a coherent cone of radiated gluons [7].

This characteristic cone becomes observable in the stream of hadrons that comprise the away-side jet. One fundamental feature of the cone is the momentum dependence of the cone's opening angle. As the momentum of the incident gluon increases, the opening angle decreases rather quickly. This feature provides a convenient method for determining whether or not the cone was produced through gluon radiation. If one observes a substantial momentum dependence of the opening angle of low-p_T hadrons, it may be the result of Cherenkov-like gluon bremsstrahlung.

2.2.4 A Flowing Cone

There is yet another way that a jet could deposit it's energy and momentum into the produced matter. In the third (and final) scenario I will discuss here, the energy from the quenched

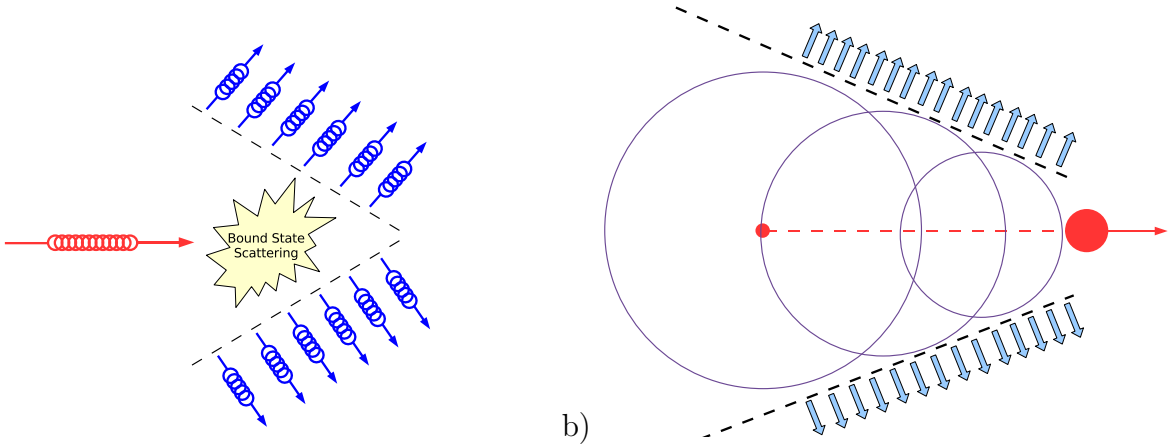

Figure 2.5: Two processes that produce a conical geometry for the away side jet. (a) Pictorial description of the scattering process that leads to gluon radiation. The incident gluon is shown in red, while the coherent radiation is in blue. In (b) a speeding parton (red) deposits it's energy into the produced matter in the form of spherical sound waves (purple). Since the parton travels faster than the speed of sound in the plasma, a Mach cone forms encouraging conical flow (blue arrows).

jet excites a collective flow in the matter, producing a sort of sub-atomic sonic boom.

When the two heavy ions collide, an assortment of $q\bar{q}$ pairs are formed throughout the fireball. As a point of illustration, we can follow a pair that is produced near the surface of the high energy density matter. As discussed previously, these pairs may result in a high-p_T particle that leaves the matter quickly, while it's companion particle is forced to traverse the majority of the fireball. Figure 2.1 may serve as a convenient reminder of this process.

As the away side jet attempts to navigate the produced matter, it deposits it's energy in the form of spherical sound waves that propagate from the instantaneous location of the quenched jet (figure 2.5). The leading parton of this jet travels with a speed very near the speed of light, while the shock wave propagates far slower at the fireball's characteristic speed of sound. It may come as no surprise that a body traveling through a medium at a speed greater than that of sound leads to conical flow behind the shock waves. This is directly analogous to the Mach cone that forms in the wake of a supersonic fighter plane.

The conical flow excited in the energetic elementary matter propagates normal to the

direction of the shock fronts, and at an angle θ_s to the hard (leading) parton (figure 2.6). When the fireball cools sufficiently, the partons trapped in the conical flow hadronize, and form mesons and baryons traveling in the same direction. It is through this mechanism that the quenched jet ultimately results in an observable cone of associated particles.

Using a simple trigonometric model, it is a straightforward manner to relate the opening angle of the cone to the speed of sound in the produced matter. Regarding figure 2.6 one can see that in the proper time interval τ the jet travels a distance $c\tau$. Additionally, the distance the shock wave travels is clearly given by

$$d_{sound} = c\tau cos\theta_s \tag{2.1}$$

where θ_s is the cone's opening angle. As the medium evolves in time, it is reasonable to assume that it's speed of sound (c_s) might as well. In this case, one can write the distance traveled by the shock wave as

$$d_{sound} = \int_0^\tau c_s(t)dt \tag{2.2}$$

comparing the two expressions for the distance traveled by the wave (2.1, 2.2) leaves an

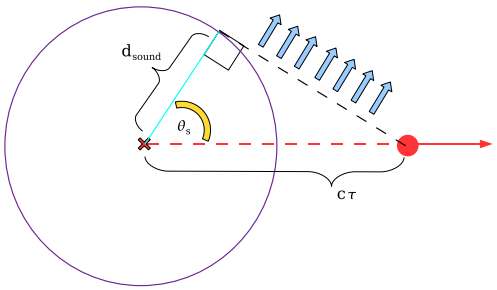

Figure 2.6: The trigonometry associated with the opening angle of the Mach cone

expression for the opening angle, it is

$$\theta_s = arccos\{\frac{1}{c\tau}\int_0^\tau c_s(t)dt\} \tag{2.3}$$

Evidently, if one can determine the correct temporal dependence of the speed of sound in the produced matter, it is possible to predict a theoretical opening angle for the cone.

One attempt at the best value for the speed of sound in the fireball considers the time-weighted average of the three stages of the produced matter's life. These stages include the quark-gluon plasma phase where $c_s \approx 1/\sqrt{3}$, the mixed phase where $c_s \approx 0$, and the resonance gas phase with $c_s \approx \sqrt{0.2}$. Completing this averaging over RHIC's data provides a value of $\langle c_s \rangle \approx 0.33$ as the most appropriate speed of sound in the produced matter [3]. Regarding (2.3) it is a simple matter to see that in this case, $\theta_s \approx 1.2$.

Like it's predecessors, this model contains a helpful characteristic that is capable of distinguishing it from other suggestions. Most notably, one can see that the value of θ_s depends only on the speed of sound in the matter, and not on the momenta of the jets (as is the case in the gluon radiation model). Accordingly, it should be true that the $\Delta\phi$ distribution is *always* peaked at $\pi \pm \theta_s$ independent of the p_T of the jet particles.

Although it is beyond the scope of this work, it is interesting to note that the presence of such collective flows may reveal some exciting properties of the produced matter. Most specifically, it has been suggested [8] that the produced matter may be a near perfect liquid. In such a substance, one would expect very low dissipation and hence the possibility for substantial collective modes such as the Mach cone.

2.3 The Grand Scheme of Things

Before embarking on an explanation of the analysis I have performed, it may be helpful to summarize this section's big ideas. Most importantly, I have introduced the study of three particle jet correlations as a reasonable method for learning about the produced matter in heavy ion collisions. Furthermore, by examining the $\Delta\phi$ distribution for these particles (figure 2.2), we have seen an interesting deviation around the away side jet. This is of particular interest because the particles in this jet interact the most with the fireball.

In an attempt to make sense of the odd away side peaks, three noteworthy models have been developed. Each of these models describes a different interaction between the partons and the plasma, and provides interesting, testable, predictions. Among these three models were the bent jet, Cherenkov-like gluon bremsstrahlung, and the Mach cone.

Determining the proper model may have substantial implications for the nature of the produced matter. If three particle correlations suggest a bent geometry, we may gain valuable information about the patterns of flow within the plasma. If the correlations describe a cone whose opening angle depends on parton p_T, there may be quark-gluon bound states in the plasma with accessible interaction strengths. Should the correlations point to a cone whose opening angle is independent of parton p_T, the resulting Mach cone may offer predictions about the time weighted speed of sound, $\langle c_s \rangle$, as well as the plasma's resistance to flow. In every case, meaningful information about the characteristics of the produced matter fall within our reach.

Chapter 3

3 Particle Correlations in PHENIX

3.1 An Analysis Overview

Once the competing mechanisms of jet modification have been described, it is possible to evaluate each through the eyes of the experiment. In this chapter I present a study of the prevailing jet geometries, the cone and the bent jet, in relation to the PHENIX detector acceptance. In the previous chapter, I noted that both the Cherenkov-like gluon bremsstrahlung and the conical flow are characterized by a tell-tale cone of secondary particles. Although the details of the cone's geometry are distinct in either scenario (the first has an opening angle that depends on p_T while the second does not), both can be simulated through common code. Furthermore, if the associated particles are all bent in the same way, it becomes a simple matter to adapt the code to describe a bent jet.

I begin by discussing the PHENIX detector acceptance, and provide a concise mini-study of the detector's influence on the two-dimensional histograms utilized in three particle correlations. After the acceptance has been successfully mapped, I develop a simple model for a modified jet in three dimensions. I show that this geometry leads to curious peaks in the $\Delta\phi$ distribution, and offer an explanation for this behavior. I conclude by summarizing

the most relevant results, and propose several steps for the evolution of this project.

3.2 Testing Our Vision

Ultimately, the physics we see is influenced heavily by the size (and shape) of the lens we see it from. It is the task of the physicist to understand this lens and correct for any aberrations. In PHENIX, where the lens is a set of limited coverage drift chambers, one must pay special attention to it's effect on angular correlations.

3.2.1 PHENIX at a Glance

It will be helpful to endure a brief orientation of the PHENIX experiment. The drift chambers that I discuss in this study surround the beam pipe with some coverage in both ϕ (the azimuthal plane perpendicular to the beam) and η. In the azimuthal plane the detector looks like two 90° segments separated by a gap of 65°. In η the detector extends to $\eta = \pm 0.3$ which corresponds to a span of about $\theta = \pi/2 \pm 1.3$ in spherical coordinates. I have provided a rendition of this set-up in figure 3.1 .

From the picture, it is clear that the detector's acceptance will play an important role in the interpretation of the $\Delta\phi$ distribution. To discover exactly *how* the acceptance influences our physics picture, it was pertinent to begin by mapping the regions of maximum and minimum acceptance in a generic correlation histogram.

3.2.2 Working With What We've Got

In this simulation, I choose three ϕ angles at random that correspond to three jet particles. The first, ϕ_1, determines the position of the high-p_T trigger, while the second and third (ϕ_2 and ϕ_3) mark the angular positions of the two secondaries. With these angles selected, I determine the angles $\Delta\phi_{12}$ and $\Delta\phi_{13}$ which correspond to the ϕ-angles separating the trigger

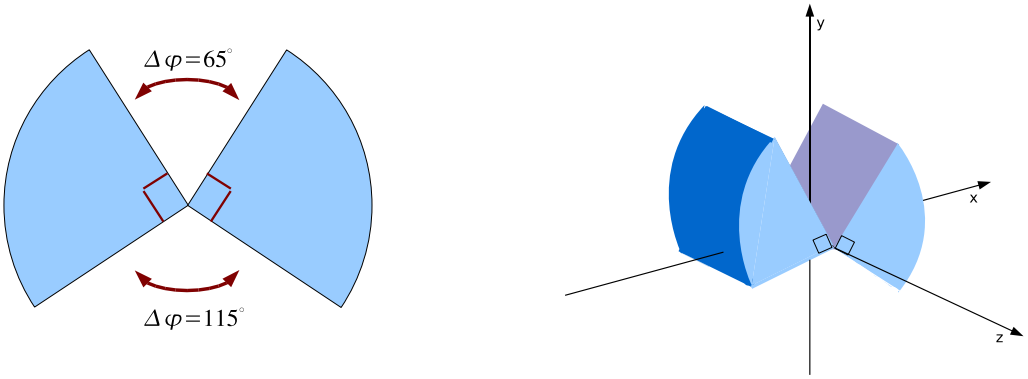

Figure 3.1: A schematic sketch of the drift chambers in the PHENIX experiment.On the left is the detector's coverage in the azimuthal plane, while the diagram at right adds the third spatial dimension.In this picture the azimuthal plane intersects the detector parallel to the light blue face, while η lies in the x-z plane. The beampipe runs along the z-axis.

particle and secondary 2 and 3, respectively. These $\Delta\phi$'s eventually make it to the two

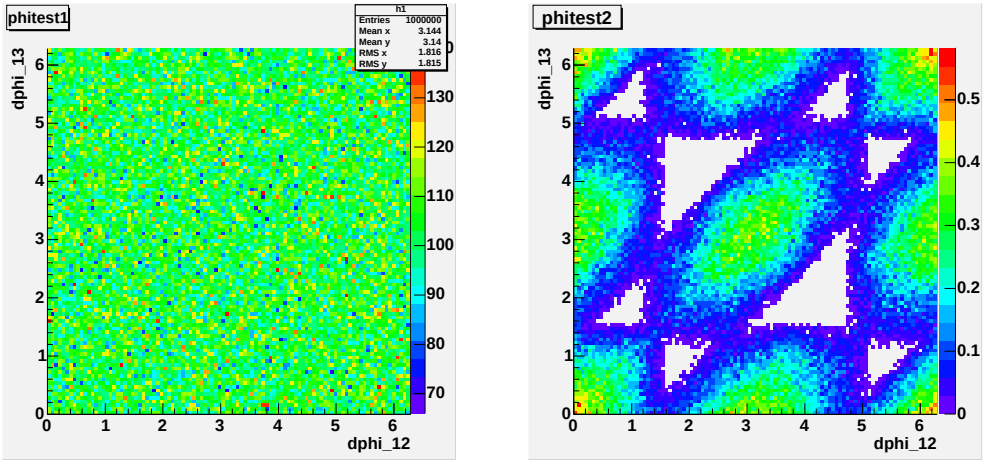

Figure 3.2: Two test histograms made to determine the detector acceptance's influence on the angular correlations. Plot at left contains all $\Delta\phi$ angles, while the one at right shows the normalized distribution after acceptance cuts were made.

dimensional histograms shown in figure 3.2. In the first plot, one can see that the distribution is statistically flat, indicating that the three particles have truly received angular positions at random. The second histogram looks far more interesting, with a series of contorted ellipses stacked upon one another. This plot is the result of applying the PHENIX detector

acceptance cuts to the generated $\Delta\phi$ angles, and normalizing with respect to the random distribution. As is evident, there is an assortment of characteristic holes and "sweet-spots" in the histogram. Furthermore, from the normalization, one can determine the relative probability of landing in any of the assorted regions.

In an attempt to provide an better understanding of exactly what constitutes a high (or low) probability event, I have provided several examples of the particle configurations in different regions of the histogram (figure 3.3). Regarding these pictures, one should note that they make good sense when viewed in the context of the detector geometry shown in figure 3.1. More specifically, the events in which two particles are on top of one another have a greater chance of being seen than those in which all three particles are separated by large angles.

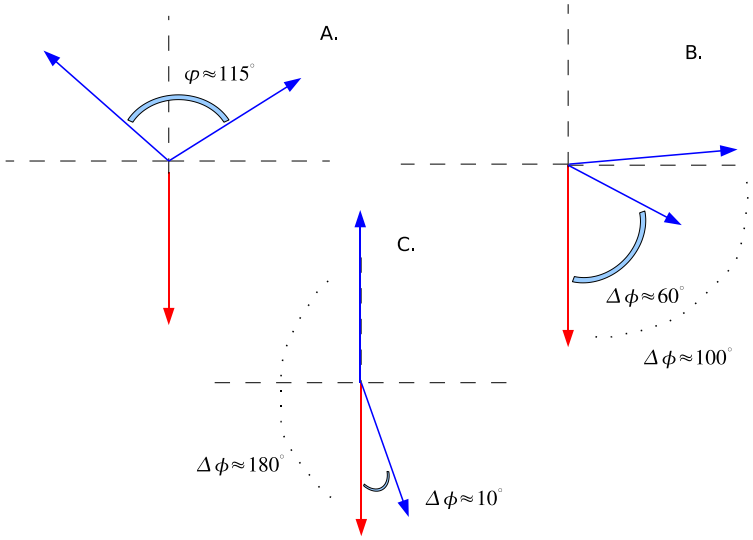

Figure 3.3: Sample configurations that illustrate unlikely (**A.** and **B.**) and likely (**C.**) events in terms of detection. **A.** corresponds to $\Delta\phi_{12} \approx 4$ and $\Delta\phi_{13} \approx 2$, **B.** occurs when $\Delta\phi_{12} \approx 1.7$ and $\Delta\phi_{13} \approx 1$, and **C.** shows $\Delta\phi_{12} \approx 0.2$ and $\Delta\phi_{13} \approx \pi$. Comparing this figure to the bottom plot in 3.2 is particularly illustrative.

Having provided a map of the detector's acceptance in three particle correlations, it is at last possible to begin exploring the consequences of different jet modifications in terms

of the $\Delta\phi$'s. In the following section I will provide a quaint picture of a cone of particles as seen by the PHENIX experiment. After these histograms have been produced, it will be possible to understand many of their features as consequences of the sweet-spots and holes shown above.

3.3 The Simple Cone

3.3.1 The Standard Configuration

To best simulate the conical geometry described by both Mach cones and gluon radiation, I settled upon a simple model consisting of a single vector in the $-\hat{z}$ direction attached at the origin to a cone opening along $\hat{z}$. In this picture, the vector along $-\hat{z}$ represents the high-p_T trigger. The fact that it has no width reflects the choice to follow just *one* particle in the nearside jet. I choose an opening angle for the cone, as well as the directions of two secondary particles that look like vectors restricted to the cone's surface. These associated particles need to cover the cone uniformly over many events, and accordingly I choose their position vectors at random.

This model aligned along the z-axis is the standard configuration in my simulation (figure 3.4). Every meaningful piece of information that precipitates from the code is a result of simple spatial rotations of the standard set-up. Because these rotations are fundamental to my analysis, I will adopt the following conventions while discussing them in this work. A rotation R of the standard configuration U_{std} clockwise around some axis a will be written

$$U' = R_{a_+} U_{std}$$

where the a_+ becomes a_- for counter clockwise rotations. A somewhat more complete exploration of the mathematical methods used here can be found in appendix A.

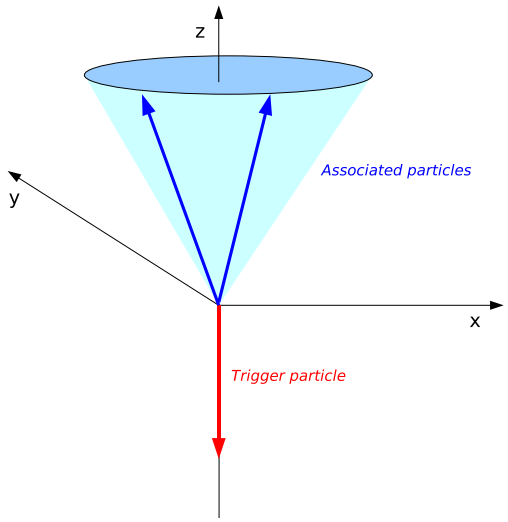

Figure 3.4: The standard configuration illustrating the geometry of my simulation. The trigger particle (red) is represented by a vector directed along $-\hat{z}$ while the secondaries (blue) are distributed randomly over the surface of a cone

Once the standard configuration has been created, it is a straight forward matter to obtain the $\Delta\phi$ angles which separate the trigger from each secondary particle. I accomplish this in part with a rotation of $\pi/2$, like $U' = R_{y_+} U_{std}$. To ensure that the rotation has been applied properly, I generate the histogram in figure 3.5. This plot shows that the associated particles have remained randomly distributed over the cone's surface. From the rotated position vectors of each of the three particles, one can determine the $\Delta\phi$ values with some simple trigonometry. Since the trigger particle has been carefully aligned with $\phi = 0$, the $\Delta\phi$ angles are simply the location in ϕ of each secondary, given by

$$\phi = arctan(y/x) \tag{3.1}$$

These angles are counted in the two dimensional histogram shown in figure 3.6.

The next step is to make the events isotropic in space. This amounts to making sure that there is no preferential orientation for the standard configuration in the coordinate system

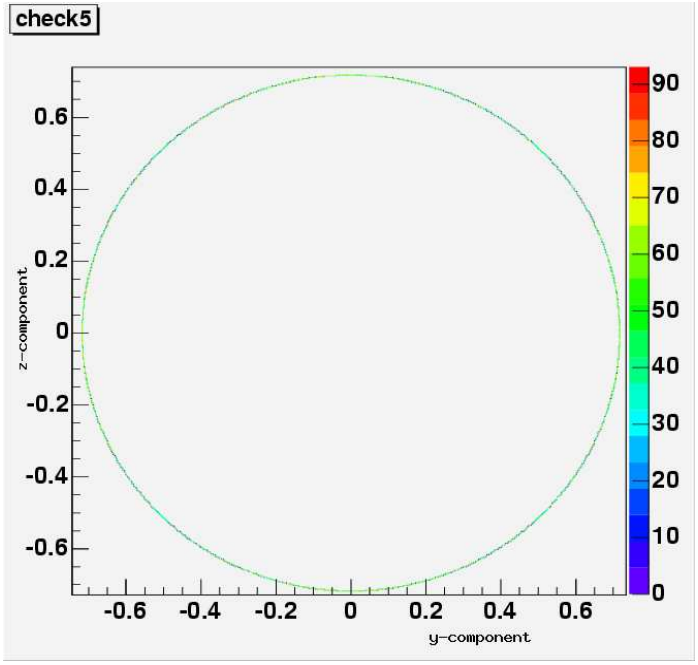

Figure 3.5: Histogram ensuring that the associated particles are distributed randomly over the surface of a cone after a rotation. The axes give the y and z components of the associated particle's location vector.

of the detector. To do this effectively, I first choose a random direction to represent the trajectory of the trigger particle. Next, I determine what rotations are needed to match the trigger particle in U_{std} with the randomly oriented trigger particle in the detector's frame. With this information, one can properly rotate the rest of U_{std} like

$$U_{det} = R_{z\_} R_{y\_} U_{std}$$

so that he is left with U_{det}, a randomly oriented conical configuration in the detector frame.

The only physics that remains to be simulated is the effect of the drift chamber's acceptance on the cone. To investigate this effect, it is necessary to first ascribe angular positions to each trajectory in U_{det} using the familiar expressions (3.1) and

$$\theta = arctan(\sqrt{x^2 + y^2}/z)$$

Once this is accomplished, one is free to apply the acceptance cuts in η and ϕ in the frame of the detector, and count the results in any number of interesting histograms.

3.3.2 The Simulation Histograms

Among the most interesting of these histograms are the ones shown in figure 3.6. On the left is a two-dimensional histogram that depicts the $\Delta\phi$ distribution before the acceptance cuts were made, while the one on the right shows the same distribution after acceptance cuts. The two histograms in figure 3.6 have a variety of notable features. First, the fact that there are only counts within a small region centered around π is illustrative of the fact that the associated particles were in fact confined to the surface of a cone. More specifically, one may notice that the region of interest (the bluish box) extends from $\pi - \phi_{open}$ to $\pi + \phi_{open}$ in both directions, where ϕ_{open} is the opening angle of the cone.

Perhaps more interestingly, the distributions are both described by an assortment of

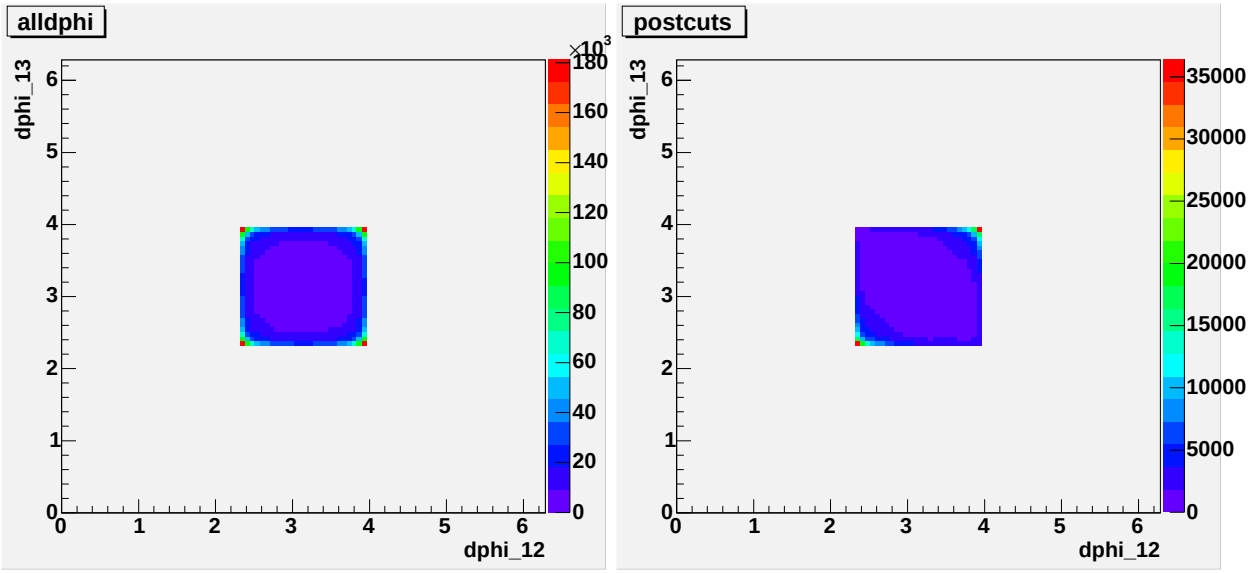

Figure 3.6: Two histograms describing a modified jet where associated particles are distributed over the surface of a cone (opening angle of 0.8 radians). On the left is before detector acceptance cuts, on the right is after.

peaks and ridges that appear along the square's perimeter. These characteristic features are quite expected, and arise as the result of a cone's map onto $\Delta\phi$ space as discussed earlier. They do not suggest that the associated particles "prefer" to travel at angles near the cone's opening angle. For a reminder of how this mapping works, it may be helpful to revisit figure 2.3. In the post acceptance cuts histogram, one can see that two of the peaks appear to have been shaved off by the acceptance. Again, this seems to be in sound agreement with what one would expect. Upon comparing the acceptance map shown in figure 3.2 to the post-cuts plot in figure 3.6, it is clear that the drift chambers in PHENIX have very poor acceptance in the regions where those two particular corners lie.

It should be noted that the histograms in figure 3.6 describe a very specific conical geometry. In these plots, the simulated cone was given an opening angle of about 46 degrees. Changing the opening angle of the cone will change both the location of the characteristic features as well as the $\Delta\phi$ distribution following the acceptance cuts. In appendix B I have provided a series of pre and post cut histograms that describe several different cones.

By dividing the post-acceptance cuts histogram by the histogram without cuts applied, one can gain some additional insight into the particulars of 3 particle correlations in PHENIX. This is shown in figure 3.7. Not surprisingly, the prominent red slash across the histogram indicates that PHENIX drift chambers are best at finding events in which the two secondaries are located in the same place. Conversely, when the associated particles are on opposite sides of the cone, there is a much smaller chance that the configuration will be detected. This observation will have a more profound impact on the case where the jet is modified to a bent geometry, and will be discussed in a later section.

In the more global context of the PHENIX experiment, the most important plots may be those that describe the cone after the detector acceptance was imposed. These histograms are indicative of what one might see in a three particle correlation of PHENIX data if the jet was indeed modified to look like a cone. By altering the cone's opening angle to better match

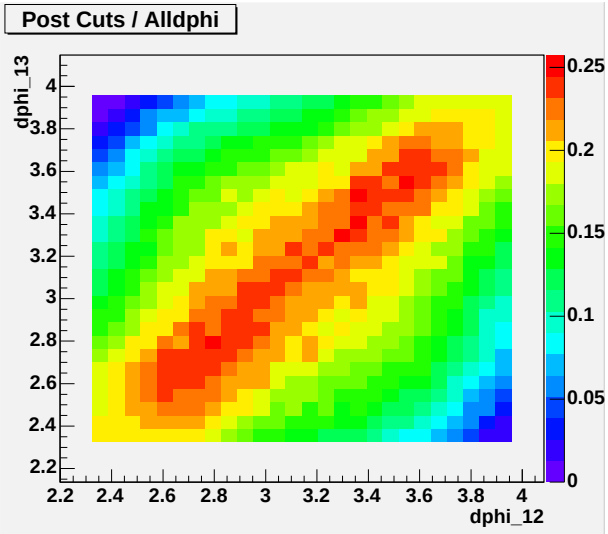

Figure 3.7: Histogram made by dividing the post acceptance cuts correlation distribution by the histogram before cuts were made. When secondaries are the same angular distance from the trigger they are more likely to be accepted by PHENIX.

the true 3 particle correlation histogram, one may have a crude means of determining an experimental opening angle. This in turn would allow one to make estimates of the speed of sound in the produced matter, or perhaps the interaction strength of partonic bound states as discussed in sections 2.2.3 and 2.2.4.

3.4 A Bent Jet Revisited

Through a simple modification of the code used to simulate a cone, it was possible to provide a quick sketch of what one might expect to see if the secondary particles were bent from the axis of the trigger particle. In the mechanism of jet bending, the most important feature is that both of the associated particles are bent in the same direction. After requiring that the two secondaries in my code satisfied this constraint, it was possible to produce the histograms shown in figure 3.8. As is evident, these distributions look very different than those which described the cone. Most notably, the square centered around π has been replaced by a segment of diagonal line. This line is a simple consequence of the fact that both particles

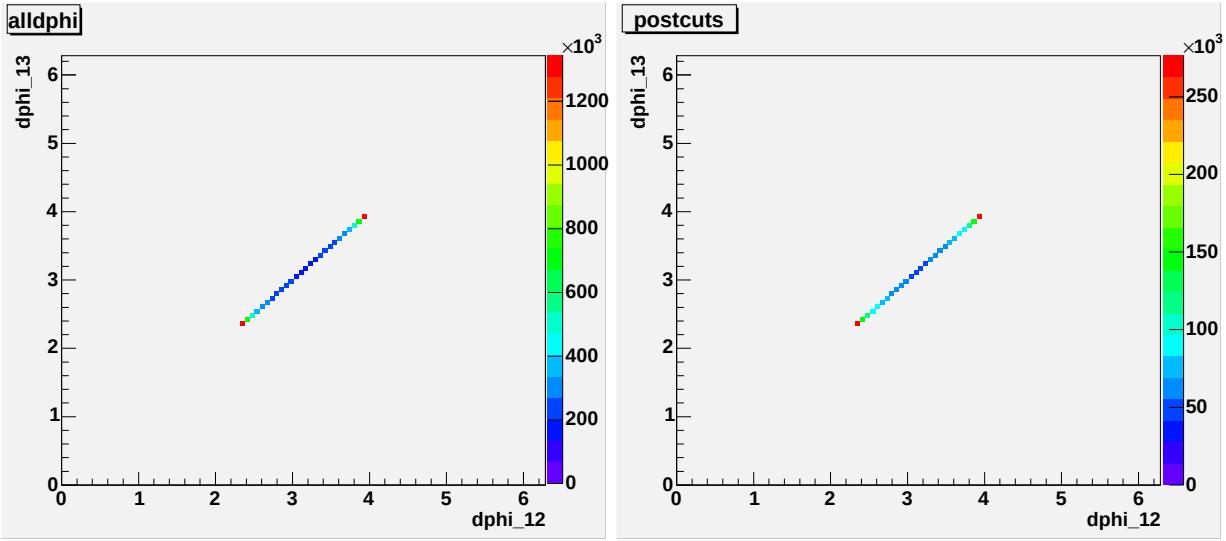

Figure 3.8: Two histograms describing a bent jet where the associated particles are bent from the trigger particles axis by 0.8 radians. On the left is before detector acceptance cuts, on the right is after.

are ending up with the same trajectory. The peaks at either end are again merely the result of a circle's appearance in $\Delta\phi$ space. Since no constraint was placed on what *direction* the jet was bent toward, over many events the secondaries trace out the surface of a cone.

One of the most interesting attributes of this plot is that PHENIX has very good (in fact its best) acceptance along the diagonal that the distribution falls on. This, coupled with the fact that the bent geometry looks markedly different from the conical geometry in three particle correlations, suggests that it may be possible to distinguish between the two geometries in the PHENIX experiment.

As a point of comparison, I have also provided a histogram that shows what happens when one divides the post acceptance cuts histogram by the pre-cut histogram (figure 3.9). This is the bent jet analogue of figure 3.7. Although the result is hardly surprising, it is worth noting that if one were to allow the bent secondary particles to be bent by slightly different amounts, the prominent diagonal would widen. This smearing could produce a distribution that resembles figure 3.7, and suggests that histograms of this kind may not be

the most effective means of distinguishing between the jet modification scenarios.

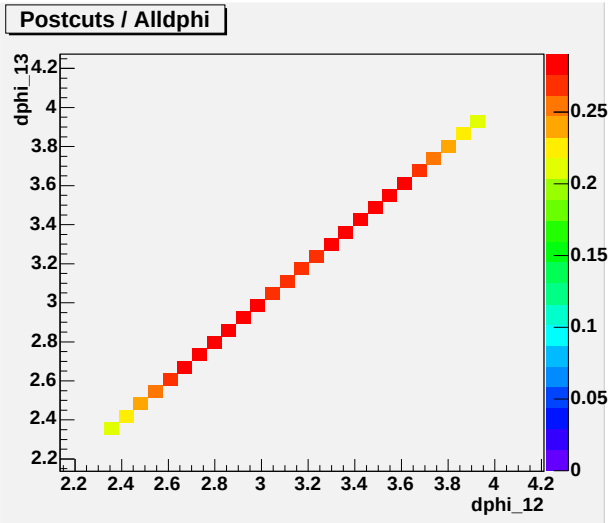

Figure 3.9: Histogram made by dividing the post acceptance cuts correlation histogram for a bent jet by the pre-cut histogram. If the associated particles are not all bent by the same amount, the diagonal line above will broaden and begin to resemble figure 3.7.

3.5 The Next Step

The simulation presented here offers a relatively terse description of the PHENIX drift chamber's acceptance on three particle correlations. Although it accomplishes what it promises to do, there are several noteworthy modifications that must be added before it has achieved maximum utility.

Fundamentally, the simulation includes a few simplifying assumptions that need not be made. The most important of these is to keep track of only one particle in the near side jet, and two in the quenched jet. In reality, there are dozens of particles in each side of the jet, and a better simulation would correlate them all. Performing these correlations will change the histograms in sections 3.3.2 and 3.4 in several significant ways. Since there will now be many particles traveling alongside the high-p_T trigger, one would expect to obtain an additional peak around $\Delta\phi = 0$ representing correlations between the trigger particle and

the others in the same jet. Also, if one gives the bent jet some "thickness" by requiring that the associated particles are bent in *approximately* the same way (to account for differing momenta, etc.) then the diagonal lines in figures 3.8 and 3.9 will broaden as well.

Chapter 4

Concluding Remarks

The study of jets in heavy ion collisions is a fascinating area of research that may provide new insight into the earliest moments of our universe's existence. Through an understanding of the ways in which a jet of hadrons is modified by the hot, dense matter produced at the center of the collision, it may be possible to discover some novel properties of a quark gluon plasma—a state of matter that hasn't existed in more than 15 billion years.

Recently, two particle angular correlations used to analyze hadron jets in the PHENIX experiment at RHIC have suggested that the produced matter does in fact alter the jets in an interesting way. In an attempt to provide a physical picture of the jet modification that agrees with the $\Delta\phi$ histogram, three distinct models have been proposed. Two of these jet modification schemes describe a conical geometry for the away side jet, while the third suggests that the associated particles are "bent" from the axis of a high-p_T trigger particle. Each of these models carries with it important consequences that could lead to increased understanding of the produced matter.

More specifically, understanding a bent jet may provide information about the flow patterns of the produced matter, while Cherenkov-like gluon bremsstrahlung may indicate the presence of partonic bound states. If the jet is modified through the existence of a Mach

cone like flow pattern, than one may be able to gain knowledge about the produced matter's characteristic speed of sound.

In an attempt to help identify which scenario is best described by the angular correlation histogram, I have presented a simulation study that offers a picture of each of the three models in terms of a three particle correlation. This technique should make it rather simple to differentiate between a bent jet and a conical geometry by following two associated particles as opposed to just one. Furthermore, I have studied the affects of the PHENIX detector acceptance on the correlation histograms, and provided a series of histograms that describe what one might see in the PHENIX experiment for each of the competing modified geometries.

These histograms show that defining features exist between a cone and a bent jet in three particle correlations, and that the acceptance of the drift chambers in PHENIX has a notable effect on the correlation histograms. Since the detectors have very good acceptance along the left-to-right diagonal, it is likely that the experiment will be able to resolve a bent jet using the three particle correlation technique. However, the existence of holes off the diagonal removes some of the defining characteristics of a conical geometry and makes it somewhat more difficult to identify.

Additionally, I have discussed the opportunities that exist for the continued evolution of this project. Although the simulation discussed in this work is complete in some sense, at present it is ignorant of some important physics that should be included. Among this physics is the fact that real jet correlations are complicated by an assortment of particles. For my simulation to be truly useful, I should include these particles in the angular correlations, which will provide a more accurate picture of the jet modification. Fortunately, implementing these changes to my code is in no way an overwhelming task, and I hope to successfully incorporate them soon.

As it stands, it is my hope that this study will find use in discussions of angular corre-

lations in the PHENIX experiment. Identifying and understanding the mechanisms of jet modification in heavy ion collisions is an important an timely pursuit that may turn out to have profound consequences. I am delighted to have had the opportunity to contribute a minuscule piece to this cosmological puzzle.

Appendix A

The Rotation Group $SO(3)$

The mathematics of spatial rotations in three dimensions is described by the special orthogonal group $SO(3)$. It is special in the sense that the 3×3 matrices that are contained in this group all have determinant one, and orthogonal in the sense that inverses of these matrices are all equal to their transposes. To see how these features arise in the study of rotations in three dimensional space, consider Euler's rotation theorem which says that any rotation can be characterized by an axis. From this, one can write a rotation in three dimensions from $u \to u'$ like

$$\begin{pmatrix} u_1' \\ u_2' \\ u_3' \end{pmatrix} = \begin{pmatrix} r_{11} & r_{12} & r_{13} \\ r_{21} & r_{22} & r_{23} \\ r_{31} & r_{32} & r_{33} \end{pmatrix} \begin{pmatrix} u_1 \\ u_2 \\ u_3 \end{pmatrix}$$

or better yet, just

$$u_i' = r_{ij} u_j$$

so long as one agrees to sum over repeated indices. Since we are rotating a vector, we know that it's length must be preserved by the rotation—that is

$$u_i' u_i' = u_i u_i \qquad \text{or} \qquad (r_{ij} u_j)(r_{ik} u_k) = u_i u_i$$

rearranging this expression gives

$$\begin{aligned} u_i u_i &= (r_{ij}u_j)(r_{ik}u_k) \\ &= r_{ij}(u_j r_{ik})u_k \\ &= r_{ij}r_{ik}u_j u_k \end{aligned}$$

which is true so long as

$$r_{ij}r_{ik} = \delta_{jk}$$

where δ_{jk} is the Kronecker delta. The above statement is known as the orthogonality condition, and it is one way of saying

$$\widetilde{R}R = 1 \qquad \text{or} \qquad R^{-1} = \widetilde{R}$$

where R is the matrix made from r_{ij}. This relationship between the transpose of a rotation matrix and it's inverse becomes particularly convenient when one wishes to change the direction of a rotation in three dimensional space. If one knows the rotation matrix for a clockwise rotation around some axis, she need only take the transpose to rotate counterclockwise about that axis.

One property of all groups is that one can form composite rotations by multiplying one group element (matrix) by another. Since the group $SO(3)$ is non-Abelian, it's members do not commute, ie.

$$R_x R_y \neq R_y R_x$$

which, in the case of this work, means that a rotation around y followed by a rotation around x does not necessarily leave one in the same place as rotating around x *then* around y.

The matrices corresponding to spatial rotations about the x, y, and z axes can be written

as

$$R_{x_+} = \begin{pmatrix} 1 & 0 & 0 \\ 0 & cos\beta & sin\beta \\ 0 & -sin\beta & cos\beta \end{pmatrix} R_{y_+} = \begin{pmatrix} cos\theta & 0 & -sin\theta \\ 0 & 1 & 0 \\ sin\theta & 0 & cos\theta \end{pmatrix} R_{z_+} = \begin{pmatrix} cos\phi & sin\phi & 0 \\ -sin\phi & cos\phi & 0 \\ 0 & 0 & 1 \end{pmatrix}$$

and, should it be of interest, the matrix that was of most importance to my simulation is just

$$R_{z_-}R_{y_-} = \begin{pmatrix} cos\theta cos\phi & -sin\phi & sin\theta cos\phi \\ cos\theta sin\phi & cos\phi & sin\theta sin\phi \\ -sin\theta & 0 & cos\theta \end{pmatrix}$$

which is the matrix used to rotate the standard configuration to the detector coordinate system from section 3.3.1.

Appendix B

$\Delta\phi$ Distribution Dependence on Cone's Opening Angle

In section 3.3.2 I mentioned that it was important to note that the angular distributions in my simulation are dependent upon α_{open}, the angle at which the cone of associated particles opens. To better illustrate this point, I have included 12 more histograms showing the $\Delta\phi$ distributions before and after the PHENIX detector acceptance cuts for $\alpha_{open} = 0.4$ to $\alpha_{open} = 1.4$ in steps of 0.2.

The most important thing to notice from this collection of histograms is the relative location of the peaks and ridges in each. Specifically, before acceptance cuts they all follow the general trends expected from the discussion in section 2.2.1, which is to say that there are peaks near the opening angles at all four corners, and ridges along the sides of the square. After detector acceptance cuts are imposed, it is interesting to observe that the number of distinguishable peaks depends heavily on the opening angle of the cone. As is evidenced by the following histograms, cones with α_{open} between 0.8 and 1.2 are left with only two easily distinguishable peaks, while cones with opening angles on either side of this range begin to show four.

$\alpha_{open} = 0.4$

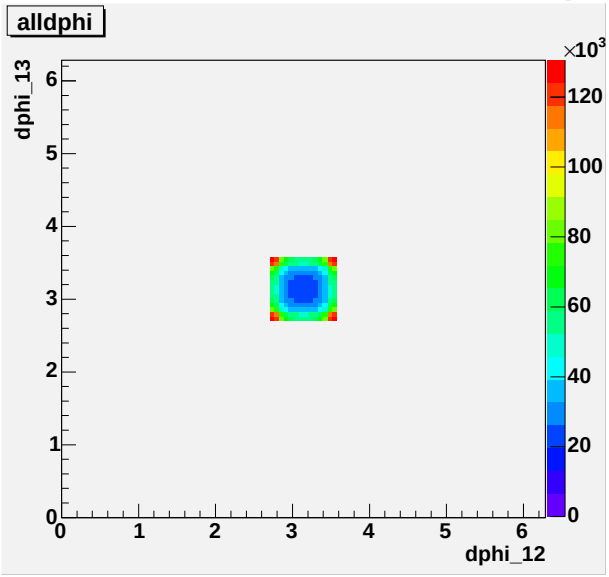

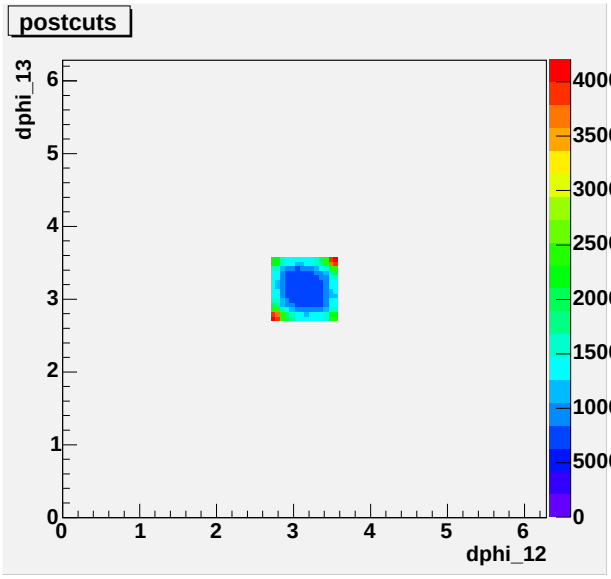

$\alpha_{open} = 0.6$

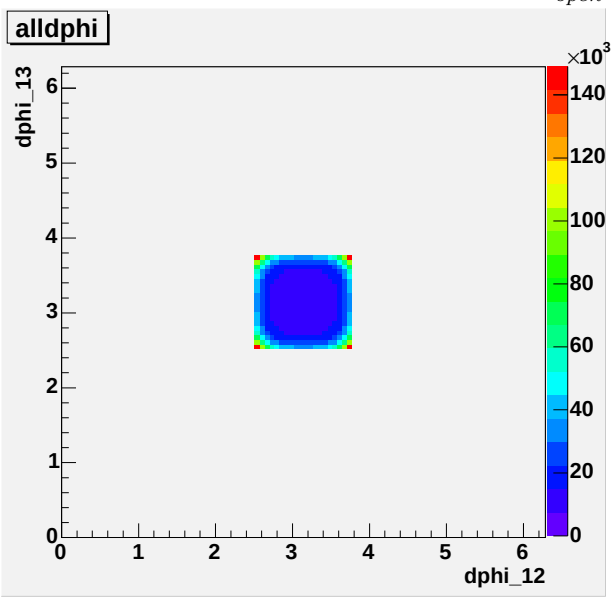

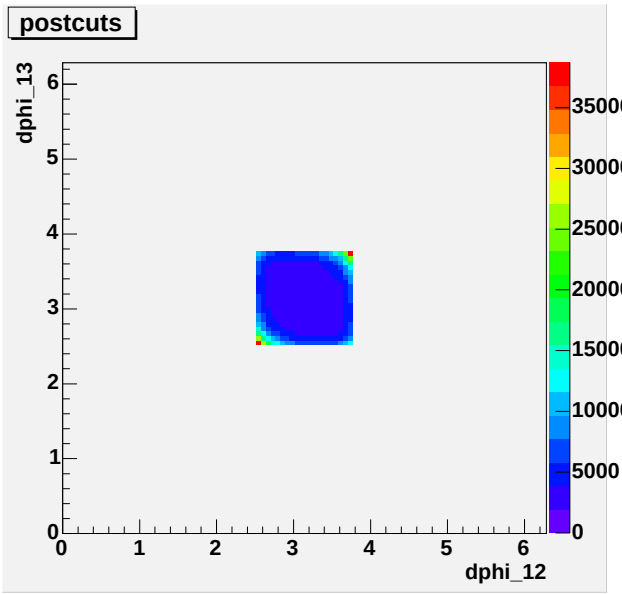

$\alpha_{open} = 0.8$

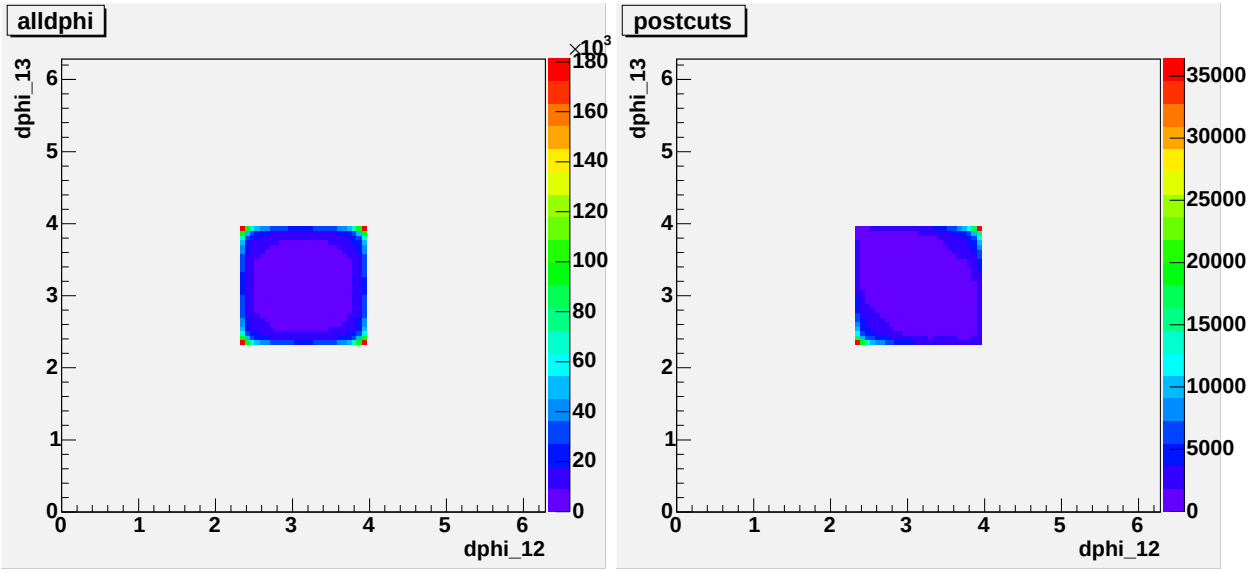

$\alpha_{open} = 1.0$

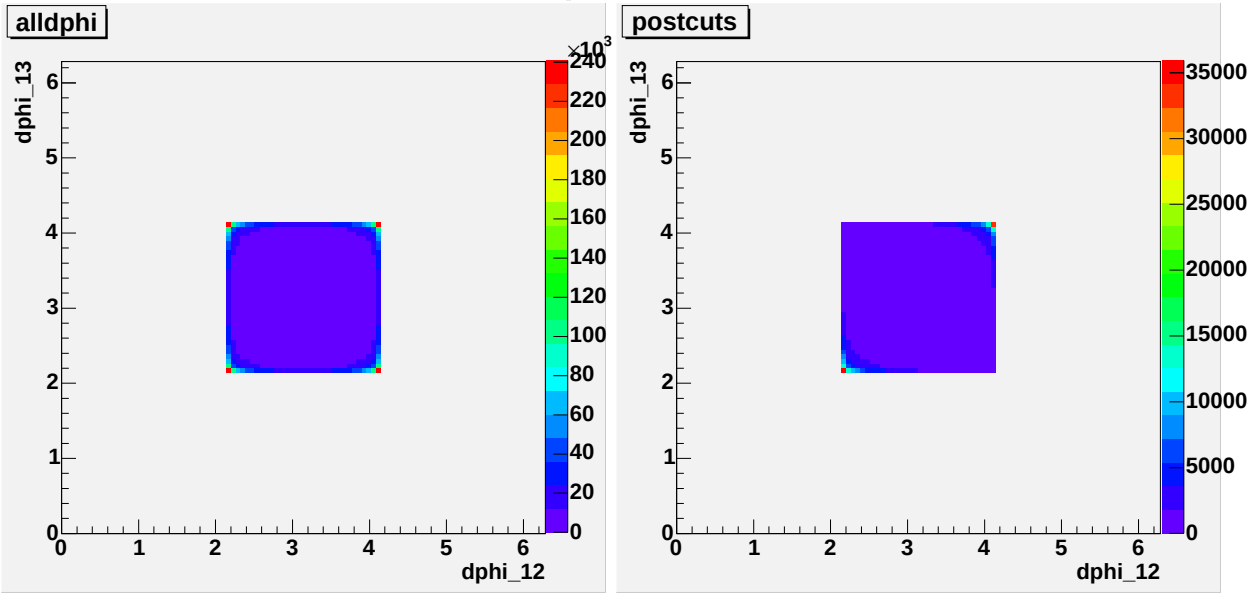

$\alpha_{open} = 1.2$

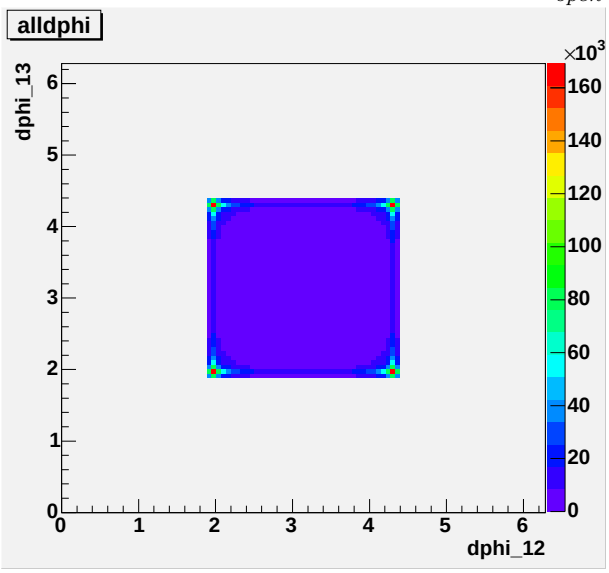

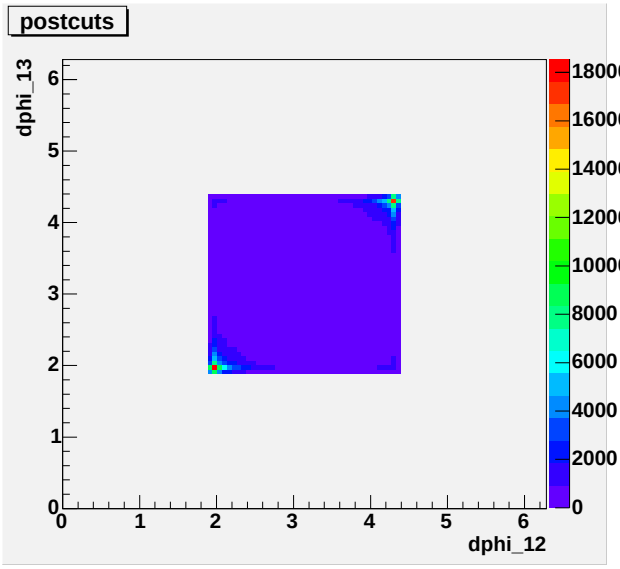

$\alpha_{open} = 1.4$

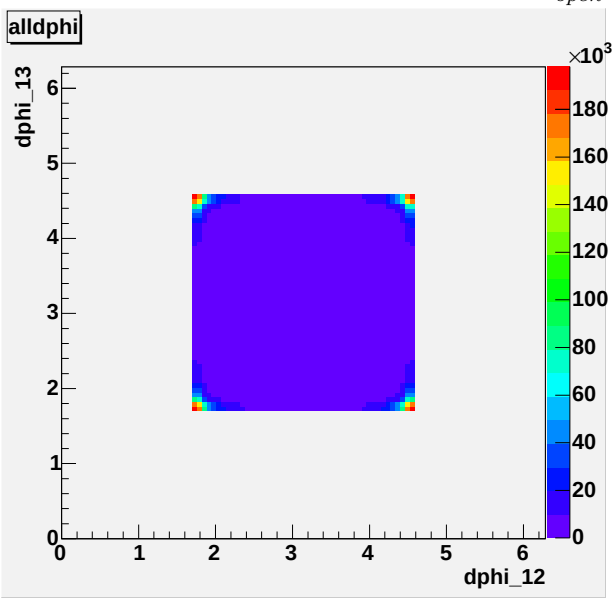

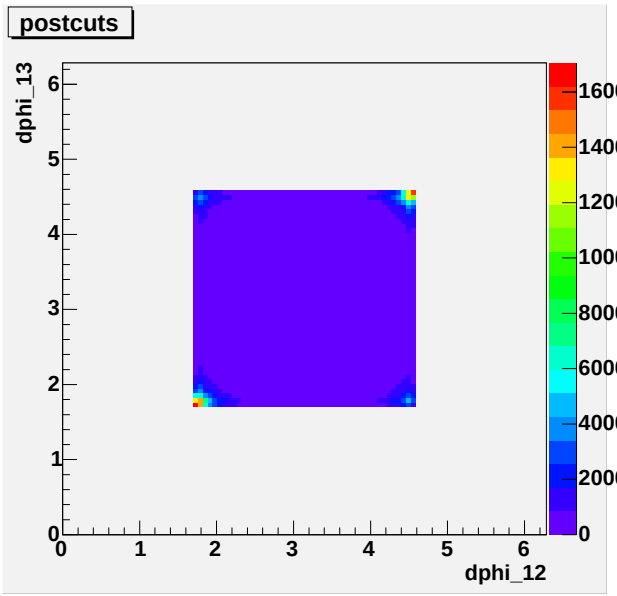

Appendix C

Mapping the Detector Acceptance

```
int phitest1();

#ifndef __CINT__
#include "TROOT.h"
#include "TFile.h"
#include "TH1.h"
#include "TH2.h"
#include "TRandom.h"
#include "TF1.h"
#include <cmath>
#include <iostream>

using namespace std;

int main()

{

  TROOT test("test","phi tests");

  return phitest1();

}

#endif
```

```
int phitest1()


{


  //gotta open a root file:

  TFile hfile("phitest1.root","RECREATE","the phi tests");

  //were gonna need to plot the differences in phi...

  TH2F*h1 = new TH2F("h1","phitest1",100,0,6.2831,100,0,6.2831);
  TH2F*h2 = new TH2F("h2","phitest2",100,0,6.2831,100,0,6.2831);
  TF1*phi = new TF1("phi","5",0,6.2831);

  for (int bin = 1; bin <=1000000; bin++)

    {

      //first get all the angles we need

      double phi1 = phi->GetRandom();
      double phi2 = phi->GetRandom();
      double phi3 = phi->GetRandom();

      //then find the differences needed being careful to redefine
      //phi1 as zero
      //each time


      double dphi12 = 0;
      double dphi13 = 0;

      if( phi1 <= phi2)
{
  dphi12 = phi2 - phi1;
}
      if( phi1 > phi2)
{
  dphi12 = 6.2831 - (phi1-phi2);
}
```

```
      if( phi1 <= phi3)
{
  dphi13 = phi3 - phi1;
}
      if( phi1 > phi3)
{
  dphi13 = 6.2831 - (phi1-phi3);
}


      //then fill the histogram with these guys

      h1 ->Fill(dphi12,dphi13);

      //we also need to see what the detector would find--taking only the
      // angles within its sight leaves

      if( ((phi1>0 && phi1<1.5707) || (phi1>2.7053 && phi1<4.2761))
 && ((phi2>0 && phi2<1.5707) || (phi2>2.7053 && phi2<4.2761)) &&
  ((phi3>0 && phi3<1.5707) || (phi3>2.7053 && phi3<4.2761)))

{

  h2 ->Fill(dphi12,dphi13);

}


    }

      //finally throw it all in a file

      cout<<"the phi test::Writing out histograms"<<endl<<endl;

      hfile.Write();
      hfile.Close();


      return 0;

}
```

Appendix D

The Primary Simulation

```
int conevec();

#ifndef __CINT__
#include "TROOT.h"
#include "TFile.h"
#include "TH1.h"
#include "TH2.h"
#include "TRandom.h"
#include "TF1.h"
#include <cmath>
#include <iostream>

using namespace std;

int main()

{


  TROOT cone("cone","simple cone2");

  return conevec();

}

#endif

int conevec()

{
```

```
  //open the root file

  TFile hfile("conevec.root","RECREATE","the simple cone2");

  //here are all the histograms and fn's needed

  double pi = acos(-1.0);
  int pick = 0;

  TF1*beta = new TF1("beta","1",0,2*pi);
  TF1*tphi = new TF1("tphi","1",0,2*pi);
  TF1*ttheta = new TF1("ttheta","sin(x)",0,pi);
  TH2F*h1 = new TH2F("h1","alldphi",100,0,2*pi,100,0,2*pi);
  TH2F*h2 = new TH2F("h2","postcuts",100,0,2*pi,100,0,2*pi);
  TH2F*h3 = new TH2F("h3","check1",1000,-2*pi,2*pi,1000,-2*pi,2*pi);
  TH1F*h4 = new TH1F("h4","dbetacut",100,0,2*pi);
  TH2F*h5 = new TH2F("h5","check2",1000,-2*pi,2*pi,1000,-2*pi,2*pi);
  TH1F*h6 = new TH1F("h6","check3",100,0,2*pi);
  TH1F*h7 = new TH1F("h7","check4",100,0,2*pi);
  TH2F*h8 = new TH2F("h8","check5",1000,-2*pi,2*pi,1000,-2*pi,2*pi);

  cout<<"Select Jet Geometry (type 0 for cone, 1 for bent)"<<endl;
  cin>>pick;
  cout<<"This will take a moment..."<<endl;

  for (int run = 1; run <= 1E7; run++)

    {


      //here, standard setup means the cone axis is along z
      //in this case the x,y,z components of secondaries look like


      double alpha = 0.8; //opening angle, can be changed to whatever
      float beta2 = beta->GetRandom(); //angle of secondary around axis
      double beta3 = beta->GetRandom();

      if (pick == 1)
{
  beta3 = beta2;
```

```
}

      h7->Fill(beta2);

      double xastd2 = sin(alpha)*cos(beta2);
      double yastd2 = sin(alpha)*sin(beta2);
      double zastd2 = cos(alpha);

      double xastd3 = sin(alpha)*cos(beta3);
      double yastd3 = sin(alpha)*sin(beta3);
      double zastd3 = cos(alpha);

      h3->Fill(xastd2,yastd2);

      //it will help to look at whats going on with the beta angles as well

      double dbeta = 0;

      if(beta2 <= beta3)
{
  dbeta = beta3-beta2;
        }
      if(beta2 > beta3)
        {
  dbeta = 2*pi - (beta2-beta3);
}

      h6->Fill(dbeta);

      //the above is the benchmark that any cone will be compared to
      //i think i can get the dphi from here if im careful...
      //the expressions below are trivial, but emphasize the rotations

      double floor = pi/2;

      double xfloor2 = xastd2*cos(floor) - zastd2*sin(floor);
      double yfloor2 = yastd2;
      double zfloor2 = xastd2*sin(floor) + zastd2*cos(floor);

      double xfloor3 = xastd3*cos(floor) - zastd3*sin(floor);
      double yfloor3 = yastd3;
      double zfloor3 = xastd3*sin(floor) + zastd3*cos(floor);
```

```
      h8->Fill(yfloor2,zfloor2);

      double phifloor2 = atan2(yfloor2,xfloor2);
      double phifloor3 = atan2(yfloor3,xfloor3);

      if(phifloor2<0)
{
  phifloor2 = 2*pi + phifloor2;
}

      if(phifloor3<0)
{
  phifloor3 = 2*pi +phifloor3;
}

      h1->Fill(phifloor2,phifloor3);

      //next lets play with the high pt trigger

      double phitrig = tphi->GetRandom();
      double thetatrig = ttheta->GetRandom();

      //here are the components of the trigger particle's vector

      double xtrig = sin(thetatrig)*cos(phitrig);
      double ytrig = sin(thetatrig)*sin(phitrig);
      double ztrig = cos(thetatrig);

      //now we can worry about the rotations
      //the simple cone axis is pi from the trigger

      double bend = pi;
      double thetarotate = (bend - thetatrig);
      double phirotate = (pi + phitrig);

      //using the appropriate rotation operator one finds

       double xarot2 = xastd2*cos(phirotate)*cos(thetarotate) -
 yastd2*sin(phirotate) + zastd2*cos(phirotate)*sin(thetarotate);
       double yarot2 = xastd2*sin(phirotate)*cos(thetarotate) +
 yastd2*cos(phirotate) + zastd2*sin(phirotate)*sin(thetarotate);
```

```
       double zarot2 = -xastd2*sin(thetarotate) + zastd2*cos(thetarotate);

       double xarot3 = xastd3*cos(phirotate)*cos(thetarotate) -
 yastd3*sin(phirotate) + zastd3*cos(phirotate)*sin(thetarotate);
       double yarot3 = xastd3*sin(phirotate)*cos(thetarotate) +
 yastd3*cos(phirotate) + zastd3*sin(phirotate)*sin(thetarotate);
       double zarot3 = -xastd3*sin(thetarotate) + zastd3*cos(thetarotate);

       //you can check that this part is working by uncommenting
       //the following lines...

       // double dot1 = (xtrig*xarot2)+(ytrig*yarot2)+(ztrig*zarot2);

       // cout<<"the dot product of the secondary and the trigger
       //is" << acos(dot1) <<endl<<endl;



       // weve now got the true vectors of the trigger and associated
       //particles
       // using this one can find their corresponding theta and phi
       //for cuts...

      double phiarot2 = atan2(yarot2,xarot2);
      double thetarot2 = atan2(sqrt((xarot2*xarot2)+(yarot2*yarot2)),
       zarot2);

      double phiarot3 = atan2(yarot3,xarot3);
      double thetarot3 = atan2(sqrt((xarot3*xarot3)+(yarot3*yarot3)),
       zarot3);

      if(phiarot2<0)
{
  phiarot2 = 2*pi + phiarot2;
}
      if(phiarot3<0)
{
  phiarot3 = 2*pi + phiarot3;
}
      if(thetarot2<0)
{
  thetarot2 = 2*pi + thetarot2;
```

```
}
      if(thetarot3<0)
{
  thetarot3 = 2*pi + thetarot3;
}

      //this should be everything


      //now lets worry about the phenix acceptance


      //in phi there are two 90deg sections separated by 65deg...
      //below are a bunch of angles that describe the detectors limits
      // in phi (should de-hardcode numbers)

      double tcut = 2*atan(exp(-0.3));

      if( ((phitrig>0 && phitrig<1.5707)||(phitrig>2.7053 &&
   phitrig<4.2761))&&
  ((phiarot2>0 && phiarot2<1.5707)||(phiarot2>2.7053 &&
     phiarot2<4.2761))&&
  ((phiarot3>0 && phiarot3<1.7507)||(phiarot3>2.7053 &&
     phiarot3<4.2761)))
{

  //now the cuts in theta

  if( (thetatrig>(pi/2)-tcut && thetatrig<(pi/2)+tcut) &&
      (thetarot2>(pi/2)-tcut && thetarot2<(pi/2)+tcut) &&
      (thetarot3>(pi/2)-tcut && thetarot3<(pi/2)+tcut))
    {
       h2->Fill(phifloor2,phifloor3);
       h4->Fill(dbeta);
       h5->Fill(xastd2,yastd2);
    }
}

    }

     //sending to file...
```

```
  cout<<"the vectorcone::Writing out histograms"<<endl<<endl;

  hfile.Write();
  hfile.Close();

  return 0;

}
```

Bibliography

[1] K. Hagiwara et al (2002), "Review of Particle Physics" Physical Review D 66, 01000

[2] K. Adcox et al (2005), "Formation of Dense Partonic Matter in Relativistic Nucleus-Nucleus Collisions at RHIC: Experimental Evaluation by the PHENIX Collaboration" nucl-ex/0410003

[3] J. Casalderrey-Solana, E.V. Shuryak, and D.Teaney (2005),"Conical Flow induced by Quenched QCD Jets" hep-ph/0411315

[4] F. Wang for the STAR collaboration, "Soft Physics from STAR—Bulk Properties", (2005).

[5] H. Busching for the PHENIX collaboration, "Highlights from the PHENIX experiment (part 2)", talk from Quark Matter (2005).

[6] Armesto, Salgado, Wiedemann (2005), "Low-p_T Collective Flow Induces High-p_T Jet Quenching" hep-ph/0411341

[7] V. Koch, A. Majunder, and Xin-Nian Wang (2005), "Cherenkov Radiation from Jets in Heavy-ion Collisions" nucl-th/0507063 v2

[8] J. Adams et al (2005), "Experimental and Theoretical Challenges in the Search for the Quark Gluon Plasma: The STAR Collaboration's Critical Assessment of the Evidence from RHIC Collisions" nucl-ex/0501009

[9] J. Ruppert and B. Muller (2005), "Waking the Colored Plasma" hep-ph/0303158

[10] T. Renk and J. Ruppert (2005), "Mach Cones in an Evolving Medium" hep-ph/0509036 v1

[11] N.N. Ajitanand for the PHENIX collaboration, "Two and Three Particle Flavor Dependent Correlations", (2005).

[12] J. Letessier and J. Rafelski: *Hadrons and Quark-Gluon Plasma*, Cambridge University Press (2002).

[13] Halzen and Martin: *Quarks & Leptons: An Introductory course in Modern Particle Physics*, Wiley (1984).

[14] G. Kane: *Modern Elementary Particle Physics*, Westview (1993).

[15] D. Griffiths: *Introduction to Elementary Particles*, Wiley (1987).

[16] F. Byron and R. Fuller: *Mathematics of Classical and Quantum Physics*, Dover (1970).

[17] H. Goldstein, C. Poole, and J. Safko: *Classical Mechanics*, Addison Wesley (2002).

[18] C. Seife: *Alpha and Omega*, Penguin (2003).